Adaptive Colour Constancy Algorithm Using Discrete Wavelet Transform

Turgay Celik, Tardi Tjahjadi
School of Engineering, University of Warwick,
Gibbet Hill Road, Coventry, CV4 7AL, United Kingdom.
Email: t.tjahjadi@warwick.ac.uk

Abstract
The colours of chromatically homogeneous object surfaces measured by a sensor vary with the illuminant colour used to illuminate the objects. In contrast, colour constancy enables humans to identify the true colours of the surfaces under varying illumination. This paper proposes an adaptive colour constancy algorithm which estimates the illuminant colour from wavelet coefficients at each scale of the decomposition by discrete wavelet transform of the input image. The angular error between the estimated illuminant colours in consecutive scales are used to determine the optimum scale for the best estimate of the true illuminant colour. The estimated illuminant colour is then used to modify the approximation subbands of the image so as to generate the illuminant-colour corrected image via inverse discrete wavelet transform. The experiments show that the colour constancy results generated by the proposed algorithm are comparable or better than those of the state-of-the-art colour constancy algorithms that use low-level image features.

Keywords:
Colour constancy, discrete wavelet transform, photometric invariance.

1. Introduction

The human visual system is able to determine with ease the colour of an object from the spectral power distribution reflected from its surface. This ability to determine a constant colour or approximately constant colour descriptor of the object irrespective of the illuminant colour illuminating the object is called colour constancy [1]. Colour constancy is essential in many colour-based computer vision applications, such as image retrieval, image classification, object recognition and object tracking [2].

Several colour constancy algorithms have been proposed and they can be categorised into two main groups. Algorithms in the first group represent images by features which are invariant with respect to the scene illuminant [3, 4], and it is not necessary to estimate the illuminant colour. Algorithms in the second group correct images for deviations from a canonical illuminant. These either propose an illuminant colour estimation and after which the image is corrected [5, 6, 4, 7], or these directly estimate the illuminant-colour corrected image [8, 9, 10] and after which the illuminant colour is determined. If desired, illuminant invariant features can be determined from the corrected image. The approach adopted in our colour constancy algorithm is of the second group.

The gamut of a canonical illuminant is the set of all possible RGB triplets, typically a white illuminant. It is represented by a convex hull in the RGB colour space [8]. Gamut mapping [8] exploits the observation that only a limited set of RGB triplets can be observed under a given illuminant, and computes the transformations that map an observed gamut into the canonical gamut in order to determine the illuminant colour. The algorithm produces among the best colour constancy results [11]. Gamut constrained illumination estimation (GCIE) algorithm [9] restricts the above-mentioned transformations to plausible existing illuminants to produce better colour constancy results. Other approaches to colour constancy include probabilistic methods [5] and learning-based methods [6]. The framework which unifies multiple colour constancy algorithms in [4] estimates the illuminant colour from the correlation of the image data and uses the prior knowledge about which colours appear under a specific illuminant.

The aforementioned colour constancy algorithms are complex and require an image dataset of known illuminants for calibration. In this paper, we focus on a colour constancy algorithm of lesser complexity and consider fast algorithms that are based on low-level image features. Max-RGB algorithm is one such algorithm which estimates illuminant colour from the maximum response of the different colour image

channels of an input image [12]. Another algorithm is based on the Grey-World algorithm [13], which assumes that the average reflectance in the scene is achromatic. Shades of Grey algorithm [14] is a general form of the Max-RGB and the Grey-World algorithms. Max-RGB algorithm is equivalent to applying the L^{∞} Minkowski norm for the error function of Shades of Grey algorithm, whereas Grey-World algorithm is equivalent to using the L^{1} norm. The best colour constancy results are obtained with the L^{6} norm. These simple colour constancy algorithms are only slightly outperformed by the more complex algorithms, e.g., gamut mapping [2, 11]. The computationally efficient algorithms such as Grey-World algorithm is embedded into the JPEG2000 coding standard [15] to achieve colour constancy. The colour constancy is applied on RGB values prior to encoding [15] which is followed by colour space transformation and encoding in discrete wavelet transform domain. Thus, computationally efficient colour constancy algorithms have potential to be applied on image/video compression technology with a moderate computational cost.

The above algorithms utilise features extracted directly from RGB values of the images. Different than the algorithms directly operating on RGB values, the gradient information of colour channels is also used for the purpose of colour constancy [10]. Grey-Edge algorithm [10] assumes that the average edge difference in the scene is achromatic and the algorithm is based on the observation that the distribution of colour derivatives exhibits the largest variation in the direction of the illuminant. The direction is approximated by the Minkowski norm of the derivatives. The algorithm is further extended to include higher-order derivatives. In the event that the gradient information of the image cannot be distinguished by a gradient operator, colour constancy cannot be provided. Another drawback of Grey-Edge algorithm is its dependency on the edge information detected by a gradient operator which in turn depends on the scale parameter of the Gaussian kernel used in the local smoothing.

Inspired by the results of Grey-Edge algorithm [10], we propose in this paper an adaptive colour constancy algorithm using discrete wavelet transform (DWT). The proposed algorithm utilizes the wavelet coefficients from the multiscale decomposition of the colour image channels via DWT to obtain estimations of the illuminant colour at different scales of the decomposition. The angular error between the illuminant colour estimations in consecutive scales is used to determine the optimum scale for estimating the true illuminant colour. The approximation subbands of the colour image channels are then modified according to the estimated illuminant colour, and are used in the inverse DWT to obtain the illuminant-colour corrected image.

The paper is organized as follows. Section 2 discusses colour constancy algorithms based on Grey-World, Max-RGB, Shades of Grey and Grey-Edge hypotheses. Section 3 presents the details of the proposed algorithm. Section 4 presents the experimental results of the proposed algorithm together with four other algorithms on two large datasets of images. Section 5 concludes the paper.

2. Colour Constancy Algorithms Based on Low-level Image Features

Using the same notation in [10], bold font to denote a vector, λ to denote wavelength, and the spatial locations of image pixels are represented by $\mathbf{x}$, the imaging of Lambertian surfaces is modelled as follows. The observed value of pixel $\mathbf{x}$, $\mathbf{p}(\mathbf{x}) = (R(\mathbf{x}), G(\mathbf{x}), B(\mathbf{x}))$, on a Lambertian surface depends on the illuminant $e(\lambda)$, the surface reflectance $r(\lambda, \mathbf{x})$, and the camera sensitivity functions $\mathbf{c}(\lambda) = (R(\lambda), G(\lambda), B(\lambda))$, and is given by [10]

$$\mathbf{p}(\mathbf{x}) = \int_{w} e(\lambda)\, r(\lambda, \mathbf{x})\, \mathbf{c}(\lambda)\, d\lambda, \tag{1}$$

where w is the visible spectrum. For imaging using only one illuminant, the colour constancy problem reduces to estimating the illuminant colour $e(\lambda)$, or its projection onto the camera sensitivity functions, given the observed image pixel values $\mathbf{p}(\mathbf{x})$, i.e.,

$$\mathbf{e} = \begin{pmatrix} R_e \\ G_e \\ B_e \end{pmatrix} = \int_{w} e(\lambda)\, \mathbf{c}(\lambda)\, d\lambda. \tag{2}$$

2.1. The Grey-World Algorithm

The Grey-World algorithm assumes that the average reflectance in a scene is achromatic [13], i.e.,

$$\frac{\int r\left(\lambda,\mathbf{x}\right)d\mathbf{x}}{\int d\mathbf{x}}=\alpha, \tag{3}$$

where the value of the constant α is between 0 for no reflectance (black) and 1 for total reflectance (white) of the incident illuminant, and the integral is over the domain of the scene. Using Eqn. (3) and Eqn. (1), and averaging over all pixel values give

$$\begin{array}{rcl}\frac{\int \mathbf{p}(\mathbf{x})d\mathbf{x}}{\int d\mathbf{x}} & = & \frac{1}{\int d\mathbf{x}}\int\int_{w} e\left(\lambda\right)r\left(\lambda,\mathbf{x}\right)\mathbf{c}\left(\lambda\right)d\lambda d\mathbf{x}\\ & = & \int_{w} e\left(\lambda\right)\left(\int\frac{r(\lambda,\mathbf{x})d\mathbf{x}}{\int d\mathbf{x}}\right)\mathbf{c}\left(\lambda\right)d\lambda\\ & = & \int_{w} e\left(\lambda\right)\alpha\mathbf{c}\left(\lambda\right)d\lambda\\ & = & \alpha\int_{w} e\left(\lambda\right)\mathbf{c}\left(\lambda\right)d\lambda\\ & = & \alpha\mathbf{e}.\end{array} \tag{4}$$

In other words, the reflected colour is equal to the illuminant colour. The normalized illuminant colour is thus given by

$$\hat{\mathbf{e}}=\alpha\mathbf{e}/\|\alpha\mathbf{e}\|. \tag{5}$$

2.2. Max-RGB Algorithm

The Max-RGB algorithm [12] assumes that the maximum reflectance which is achieved for each of the three colour image channels is equal, i.e.,

$$\begin{array}{rcl}\max\limits_{\mathbf{x}}\ \mathbf{p}\left(\mathbf{x}\right) & = & \left(\max\limits_{\mathbf{x}}\ R\left(\mathbf{x}\right),\max\limits_{\mathbf{x}}\ G\left(\mathbf{x}\right),\max\limits_{\mathbf{x}}\ B\left(\mathbf{x}\right)\right)\\ & = & \alpha\mathbf{e},\end{array} \tag{6}$$

where the max operation is applied to the separate channels. The maxima of the separate channels do not have to be on the same location, thus the algorithm also obtains correct illuminant colour estimation when the maximum reflectance is equal for the three channels [10].

2.3. Shades of Grey Algorithm

Shades of Grey algorithm [14] is a reformulation of Eqn. (4) according to the Minkowski norm to give

$$\left(\frac{\int \mathbf{p}^{k}\left(\mathbf{x}\right)d\mathbf{x}}{\int d\mathbf{x}}\right)^{1/k}=\alpha\mathbf{e}, \tag{7}$$

where $k\in\mathbb{R}$. The Grey-World and Max-RGB formulations respectively given in Eqn. (4) and Eqn. (6) are instantiations of Shades of Grey algorithm for $k=1$ and $k=\infty$, respectively. It has been shown that the best colour constancy results are obtained with $k=6$ [14].

2.4. Grey-Edge Algorithm

The Grey-Edge algorithm [10] assumes that the average of the reflectance differences in a scene is achromatic, i.e.,

$$\frac{\int \left|r_{\mathbf{x}}^{\sigma}\left(\lambda,\mathbf{x}\right)\right|d\mathbf{x}}{\int d\mathbf{x}}=\alpha, \tag{8}$$

where σ is a scale operator which is the standard deviation of the Gaussian filter used in local smoothing, $|\cdot|$ is the absolute value operator, and the subscript $\mathbf{x}$ indicates spatial derivative. The scene illuminant colour is computed from the average colour derivative in the image [10], i.e.,

$$\begin{array}{rcl} \frac{\int |\mathbf{p}^{\sigma}_{\mathbf{x}}(\mathbf{x})| d\mathbf{x}}{\int d\mathbf{x}} & = & \frac{1}{\int d\mathbf{x}} \int \int_{w} e(\lambda) |r^{\sigma}_{\mathbf{x}}(\lambda, \mathbf{x})| \mathbf{c}(\lambda) d\lambda d\mathbf{x} \\ & = & \int_{w} e(\lambda) \left(\int \frac{|r^{\sigma}_{\mathbf{x}}(\lambda, \mathbf{x})| d\mathbf{x}}{\int d\mathbf{x}} \right) \mathbf{c}(\lambda) d\lambda \\ & = & \int_{w} e(\lambda) (\alpha) \mathbf{c}(\lambda) d\lambda \\ & = & \alpha \int_{w} e(\lambda) \mathbf{c}(\lambda) d\lambda \\ & = & \alpha \mathbf{e}, \end{array} \tag{9}$$

where $|\mathbf{p}^{\sigma}_{\mathbf{x}}| = (|R^{\sigma}_{\mathbf{x}}|, |G^{\sigma}_{\mathbf{x}}|, |B^{\sigma}_{\mathbf{x}}|)$.

The Grey-Edge algorithm can be adapted to incorporate the Minkowski norm as follows [10]:

$$\left(\frac{\int |\mathbf{p}^{\sigma}_{\mathbf{x}}|^{k} (\mathbf{x}) d\mathbf{x}}{\int d\mathbf{x}} \right)^{1/k} = \alpha \mathbf{e}, \tag{10}$$

assuming that the k-th Minkowski norm of the derivative of the reflectance in a scene is achromatic. Note that when $k = 1$, the illuminant colour is determined by an averaging operation over the derivatives of the channels. When $p = \infty$, the illuminant colour is computed from the maximum derivative. Note also the similarity between the derivations of colour constancy from Grey-World and Grey-Edge hypotheses. Eqn. (10) can be generalized by considering higher order spatial derivatives [10], i.e.,

$$\left(\frac{\int |\frac{\partial^{n} \mathbf{p}^{\sigma}(\mathbf{x})}{\partial \mathbf{x}^{n}}|^{k} d\mathbf{x}}{\int d\mathbf{x}} \right)^{1/k} = \alpha \mathbf{e}, \tag{11}$$

but the best performance is obtained using the first order partial derivatives [10].

3. Proposed Algorithm

An image $\mathbf{p}$ can be decomposed into its approximation ($\mathbf{p}_{l} = l(\mathbf{p})$) and detail ($\mathbf{p}_{h} = h(\mathbf{p})$) components by using a set of appropriate spatial lowpass filter (l) and highpass filter (h), i.e.,

$$\mathbf{p}(\mathbf{x}) = \mathbf{p}_{l}(\mathbf{x}) + \mathbf{p}_{h}(\mathbf{x}), \tag{12}$$

where the filtering operation is applied to the lattice of the image. By considering that the filtering operation is applied along the spatial neighbourhood of pixel $\mathbf{x}$, and using Eqn. (1) together with Eqn. (12) one can derive

$$\begin{array}{rcl} \mathbf{p}_{l}(\mathbf{x}) & = & l\left(\int_{w} e(\lambda) r(\lambda, \mathbf{x}) \mathbf{c}(\lambda) d\lambda \right) \\ & = & \int_{w} e(\lambda) l(r(\lambda, \mathbf{x})) \mathbf{c}(\lambda) d\lambda \\ & = & \int_{w} e(\lambda) r_{l}(\lambda, \mathbf{x}) \mathbf{c}(\lambda) d\lambda, \end{array} \tag{13}$$

$$\begin{array}{rcl} \mathbf{p}_{h}(\mathbf{x}) & = & h\left(\int_{w} e(\lambda) r(\lambda, \mathbf{x}) \mathbf{c}(\lambda) d\lambda \right) \\ & = & \int_{w} e(\lambda) h(r(\lambda, \mathbf{x})) \mathbf{c}(\lambda) d\lambda \\ & = & \int_{w} e(\lambda) r_{h}(\lambda, \mathbf{x}) \mathbf{c}(\lambda) d\lambda, \end{array} \tag{14}$$

where $r_{l}(\lambda, \mathbf{x})$ and $r_{h}(\lambda, \mathbf{x})$ are respectively the approximation and detail components of reflectance $r(\lambda, \mathbf{x})$. Thus, separating the image into approximation and detail components also separates the scene reflectance into the corresponding components.

Like the Grey-World algorithm, the proposed algorithm assumes that the average of details of reflectance in a scene is achromatic, i.e.,

$$\frac{\int |r_{h}(\lambda, \mathbf{x})| d\mathbf{x}}{\int d\mathbf{x}} = \alpha. \tag{15}$$

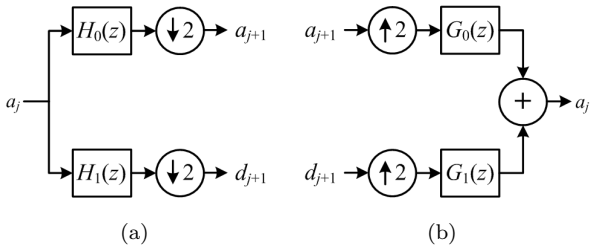

Figure 1: Structure of the 1D DWT filter bank: $H_n(z)$ and $G_n(z)$ are digital filters; a_n and d_n are respectively the scaling coefficients and wavelet coefficients; n are integer indices; and down-arrow and up-arrow are respectively downsampling and upsampling operations.

Using Eqn. (14) together with Eqn. (15), the illuminant colour is estimated as follows:

$$\begin{array}{rcl} \frac{\int |\mathbf{p}_h(\mathbf{x})| d\mathbf{x}}{\int d\mathbf{x}} & = & \frac{1}{\int d\mathbf{x}} \int \int_w e(\lambda) |r_h(\lambda, \mathbf{x})| \mathbf{c}(\lambda) d\lambda d\mathbf{x} \\ & = & \int_w e(\lambda) \left(\int \frac{|r_h(\lambda, \mathbf{x})| d\mathbf{x}}{\int d\mathbf{x}} \right) \mathbf{c}(\lambda) d\lambda \\ & = & \int_w e(\lambda) (\alpha) \mathbf{c}(\lambda) d\lambda \\ & = & \alpha \int_w e(\lambda) \mathbf{c}(\lambda) d\lambda \\ & = & \alpha \mathbf{e}, \end{array} \tag{16}$$

where $|\mathbf{p}_h(\mathbf{x})| = (|R_h(\mathbf{x})|, |G_h(\mathbf{x})|, |B_h(\mathbf{x})|)$.

Like Shades of Grey and Grey-Edge algorithms, the proposed algorithm can also be adapted to incorporate the Minkowski norm, i.e.,

$$\left(\frac{\int |\mathbf{p}_h(\mathbf{x})|^k d\mathbf{x}}{\int d\mathbf{x}} \right)^{1/k} = \alpha \mathbf{e}. \tag{17}$$

The colour constancy based on (17) assumes that the k-th Minkowski norm of the details in a scene is achromatic.

The approximation and detail components are computed using DWT. Specifically, the non-redundant DWT is employed to separate the image into approximation and detail subbands at different scales of the decomposition. The one-dimensional (1D) DWT decomposes a signal $p(t) \in L^2(\mathbb{R})$ in terms of a shifted and dilated scaling function $\phi(t)$, and mother wavelet $\psi(t)$, i.e.,

$$p(t) = \sum_{k \in \mathbb{Z}} a_{j_0,k} \phi_{j_0,k}(t) + \sum_{j \geq j_0} \sum_{k \in \mathbb{Z}} d_{j,k} \psi_{j,k}(t) \tag{18}$$

where $\phi_{j_0,k}(t) \equiv 2^{j_0/2} \phi\left(2^{j_0} t - k\right)$ and $\psi_{j,k}(t) \equiv 2^{j/2} \psi\left(2^j t - k\right)$ [16]. The scaling coefficients $a_{j_0,k}$ and wavelet coefficients $d_{j,k}$ can be computed using the standard L^2 inner product when the set $\{\phi_{j_0,k}, \psi_{j,k}, j \geq j_o, k \in \mathbb{Z}\}$ forms an orthonormal basis for $L^2(\mathbb{R})$, i.e., $a_{j_0,k} = \langle p, \phi_{j_0,k} \rangle$, and $d_{j,k} = \langle p, \psi_{j,k} \rangle$.

The DWT is computed recursively using the filter bank structure shown in Fig. 1(a). The scaling coefficients at scale j $\{a_{j,k}, k \in \mathbb{Z}\}$ are used to compute the scaling coefficients $\{a_{j+1,k}, k \in \mathbb{Z}\}$ and wavelet coefficients $\{d_{j+1,k}, k \in \mathbb{Z}\}$ at scale $j+1$ by passing $\{a_{j,k}\}$ through digital filters $H_0(z)$ and $H_1(z)$, and downsampling by a factor of two. The impulse responses $h_0[n]$ and $h_1[n]$ of $H_0(z)$ and $H_1(z)$, respectively, are related to the scaling and wavelet basis functions in (18) by $\phi(t) = \sqrt{(2)} \sum_n h_0[n] \phi(2t - n)$, and $\psi(t) = \sqrt{(2)} \sum_n h_1[n] \phi(2t - n)$ [17]. To reconstruct the signal from its wavelet (and scaling) coefficients, we apply the filter bank structure shown in Fig. 1(b), which computes the scaling coefficients $a_{j,k}$ at scale j by upsampling $a_{j+1,k}$ and $d_{j+1,k}$, filtering respectively with $G_0(z)$ and $G_1(z)$ (whose impulse responses are the time reversed versions of h_0 and h_1 in the orthogonal case), and adding the results.

The 2-dimensional (2D) DWT decomposes an image $p(\mathbf{x}) \in L^2(\mathbb{R}^2)$ in terms of a set of shifted and dilated wavelet functions $\{\psi^{0^\circ}, \psi^{90^\circ}, \psi^{\pm 45^\circ}\}$ and scaling function $\phi(\mathbf{x})$, i.e.,

$$p(\mathbf{x}) = \sum_{k \in \mathbb{Z}^2} a_{j_0,k} \phi_{j_0,k}(\mathbf{x}) + \sum_{b \in \mathcal{B}} \sum_{j \geq j_0} \sum_{k \in \mathbb{Z}^2} d^b_{j,k} \psi^b_{j,k}(\mathbf{x}) \tag{19}$$

where $\phi_{j_0,k}(\mathbf{x}) \equiv 2^{j_0} \phi\left(2^{j_0}\mathbf{x} - k\right)$, $\psi^b_{j,k}(\mathbf{x}) \equiv 2^j \psi^b\left(2^j \mathbf{x} - k\right)$, and $b \in \mathcal{B} \equiv \{\psi^{0^\circ}, \psi^{90^\circ}, \psi^{\pm 45^\circ}\}$ are the wavelet subbands of the DWT decomposition. For separable 2D DWT, $\psi^{0^\circ}(\mathbf{x}) \equiv \psi^{0^\circ}(x_1, x_2) = \phi(x_1)\psi(x_2)$, $\psi^{90^\circ}(\mathbf{x}) \equiv \psi^{90^\circ}(x_1, x_2) = \psi(x_1)\phi(x_2)$, and $\psi^{\pm 45^\circ}(\mathbf{x}) \equiv \psi^{\pm 45^\circ}(x_1, x_2) = \psi(x_1)\psi(x_2)$, where ϕ, ψ are 1D scaling and wavelet functions as in (18), and x_1, x_2 are components of 2D spatial location $\mathbf{x}$, i.e., $\mathbf{x} = (x_1, x_2)$. A separable 2D DWT can be computed efficiently in discrete time by applying the associated 1D filter bank to each column of the image, and then applying the filter bank to each row of the result. Thus, one can consider wavelets as local edge detectors in the horizontal (0° subband), vertical (90°) and diagonal (±45°) directions at different scales.

A J-level DWT decomposition of an image p produces a set of wavelet subbands $\left\{\psi^{0^\circ}_j, \psi^{90^\circ}_j, \psi^{\pm 45^\circ}_j\right\}$ at each level j, where $j = 1, \ldots, J$, and an approximation subband ϕ_J at the final level J. The original image p can be perfectly reconstructed from its J-level DWT decomposition using the approximation subband ϕ_J at the final level and sets of wavelet subbands $\left\{\psi^{0^\circ}_j, \psi^{90^\circ}_j, \psi^{\pm 45^\circ}_j\right\}$, $j = 1, \ldots, J$. The wavelet subbands $\left\{\psi^{0^\circ}_J, \psi^{90^\circ}_J, \psi^{\pm 45^\circ}_J\right\}$ and approximation subband ϕ_J at the final level J are used to create an approximation subband ϕ_{J-1} at the scale $J-1$. This procedure is recursively repeated until the image is reconstructed completely.

For a given 2D image p and its wavelet subbands $\left\{\psi^{0^\circ}_j, \psi^{90^\circ}_j, \psi^{\pm 45^\circ}_j\right\}$ for $j = 1, \ldots, J$ resulted from J-level DWT decomposition, the detail component p^j_h of p at scale j is estimated from the wavelet subbands as

$$p^j_h = \sqrt{\left(\psi^{0^\circ}_j\right)^2 + \left(\psi^{90^\circ}_j\right)^2 + \left(\psi^{\pm 45^\circ}_j\right)^2}. \tag{20}$$

Thus, the illuminant colour estimation $\mathbf{e}_j$ at scale j can be calculated using the (17) and (20) as

$$\left(\frac{\int |\mathbf{p}^j_h(\mathbf{x})|^k d\mathbf{x}}{\int d\mathbf{x}}\right)^{1/k} = \alpha_j \mathbf{e}_j, \tag{21}$$

where $\alpha_j \in \mathbb{R}$, $\mathbf{e}_j \in \mathbb{R}^3$, and $|\mathbf{p}^j_h(\mathbf{x})| = \left(|R^j_h(\mathbf{x})|, |G^j_h(\mathbf{x})|, |B^j_h(\mathbf{x})|\right)$.

There will be a total of J estimations of the illuminant colour resulted from J-level DWT decomposition. However, selecting the correct estimation is not trivial. When the wavelet coefficients at finer scale $j-1$ provides statistically strong features for illuminant colour estimation, due to the nature of discrete wavelet transform, one expects the similar estimation at very coarse scale j. Meanwhile, the estimation in finer scale is more prone to errors caused from fluctuations on wavelet coefficients. Due to multiscale decomposition, it is expected that the illuminant colour estimation at scale j is similar to the estimation at scale $j-1$. Thus the difference in illuminant colour estimations between consecutive scales can be used to select the optimum scale where the estimations in consecutive scales, i.e., j and $j-1$, have minimum angular error. The difference $\delta_{j,j-1}$ between two normalized illuminant colour estimations $\hat{\mathbf{e}}_j$ and $\hat{\mathbf{e}}_{j-1}$ from scales j and $j-1$, respectively, can be measured using the angular error

$$\delta_{j,j-1} = \Delta\theta(\hat{\mathbf{e}}_j, \hat{\mathbf{e}}_{j-1}) = \arccos(\hat{\mathbf{e}}_j \cdot \hat{\mathbf{e}}_{j-1}), \tag{22}$$

where $(\hat{\mathbf{e}}_j \cdot \hat{\mathbf{e}}_{j-1})$ is the dot product of $\hat{\mathbf{e}}_j$ and $\hat{\mathbf{e}}_{j-1}$, and $\delta_{1,0} = \delta_{1,J}$. Using the consecutive illuminant colour estimation differences $\delta_{j,j-1}$ for $j = 1, \ldots, J$, the optimum scale j_o is selected according to the minimum estimation difference

$$j_o = \underset{j \in \{1,\ldots,J\}}{\arg\min}\ \delta_{j,j-1} \tag{23}$$

and the normalized true illuminant colour $\hat{\mathbf{e}}$ is estimated using the optimum scale j_o as

$$\hat{\mathbf{e}} = \hat{\mathbf{e}}_{j_o}. \tag{24}$$

Colour constancy algorithms modify the colour image channels according to the normalized illuminant colour. This operation is carried out on the full image lattice, and requires a large amount of division operations. Unlike the other colour constancy algorithms, the proposed algorithm only modifies the approximation subbands at the coarsest level (i.e., the final level) of the colour image channels resulted from J-level DWT decompositions according to estimated illuminant colour in (24), i.e.,

$$\begin{array}{rcl} \phi_J^R & \Leftarrow & \phi_J^R / \left(\sqrt{3}\hat{\mathbf{e}}_{j_o}^R\right), \\ \phi_J^G & \Leftarrow & \phi_J^G / \left(\sqrt{3}\hat{\mathbf{e}}_{j_o}^G\right), \\ \phi_J^B & \Leftarrow & \phi_J^B / \left(\sqrt{3}\hat{\mathbf{e}}_{j_o}^B\right), \end{array} \tag{25}$$

where ϕ_J^p, $p \in \{R, G, B\}$, is the approximation subband resulted from J-level DWT decomposition of colour image channel p, and $\hat{\mathbf{e}}_{j_o}^p$ is the component of $\hat{\mathbf{e}}_{j_o}$ that belongs to the colour image channel p. Using the updated approximation subband ϕ_J^p according to (25) and the corresponding wavelet subbands, the illuminant-colour corrected image is reconstructed using the inverse DWT. The main advantage of the proposed algorithm is its efficient computational structure.

The maximum DWT decomposition levels, J, of an $a \times b$ input image is given by

$$J = \min\left(\lfloor \log_2(a/8) \rfloor, \lfloor \log_2(b/8) \rfloor\right), \tag{26}$$

where $\lfloor\ \rfloor$ rounds the input parameter toward the lowest integer number. The factor 8 defines the smallest size of the approximation subband. It is found experimentally that using a factor smaller than 8 produces visual artifacts in the reconstructed image.

4. Experiments

The performances of the proposed and four other colour constancy algorithms of similar complexity are evaluated for various parameter settings on a dataset of images of colourful objects under a controlled indoor setting, and on a real-world dataset containing images of mainly outdoor scenes. For both datasets, the illuminant colours of the scenes are provided as additional information (i.e., ground truths).

In the experiments, the angular error $\Delta\theta$ computed according to (22) between the estimated normalized illuminant colour $\hat{\mathbf{e}}_e$ and the normalized actual illuminant colour $\hat{\mathbf{e}}_a$ is used as an error measure. For the two datasets, the median angular error is considered to be appropriate for assessing the performance of colour constancy algorithms [18, 10]. We used the implementations of Grey-World, Max-RGB, Shades of Grey and Grey-Edge algorithms available from [10]. Furthermore, the Daubechies (db) wavelet filters with different lengths are used to study the effects of employing different lengths of wavelet filters on colour constancy.

4.1. Quantitative Assessment

4.1.1. Controlled Indoor Dataset

The colour constancy algorithms are first evaluated on a dataset [19] of 530 images of colourful objects, with either matte or specular surfaces, captured under different illuminants. All the objects are placed on a dark background, and the pose of each object is changed whenever the illuminant is changed. Some sample images from the indoor dataset [19] are shown in Fig. 2.

Different parameter settings of Shades of Grey, Grey-Edge, and the proposed algorithms give different colour constancy results. The dependency of median angular error on different parameters of the algorithms is shown in Fig. 3, where as expected the Minkowski norm has the highest influence on the performance of the different algorithms. For example, the wavelet coefficients employed in the proposed algorithm to estimate the illuminant colour have values ranging from small to large. The small values are generally insignificant and are mainly due to the noise inherent in images. The large values on the other hand have the major

Figure 2: Sample images from the controlled indoor dataset [19].

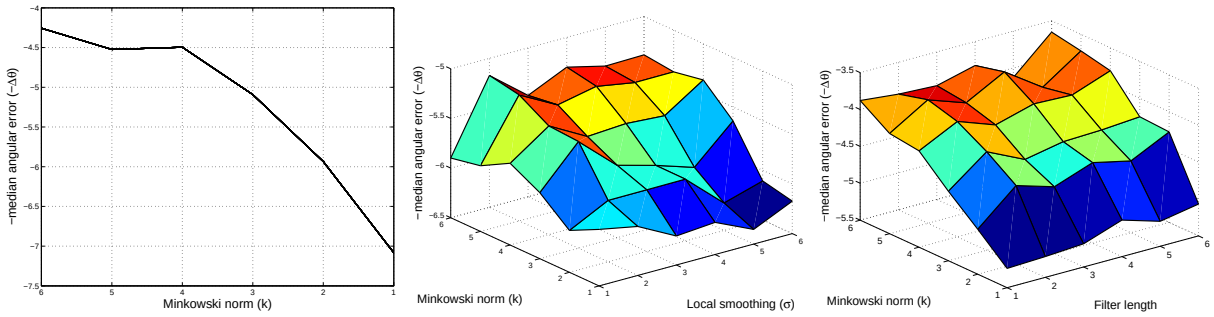

(a) (b) (c)

Figure 3: Dependency of median angular error on parameter settings of the colour constancy algorithms on the controlled indoor dataset [19]: (a) Shades of Grey; (b) Grey-Edge; and (c) the proposed algorithm. The angular error axis is inverted for visualization purpose. Since Shades of Grey algorithm is only dependent on Minkowski norm k, both the x- and y-axis of Shades of Grey graph refer to the Minkowski norm.

Table 1: Performances of different colour constancy algorithms in term of median angular error (in degrees) on the controlled indoor dataset.

Method	Median Angular Error
Grey-World	7.08
Max-RGB	6.74
Shades of Grey	4.26
Grey-Edge	5.17
Proposed	3.65

influence on estimating the correct illuminant colour. The higher values of Minkowski norm suppress the small coefficient values while further enhance the large coefficient values. Thus significant number of high coefficient values are automatically selected. As a result, the higher values of Minkowski norm results in better performances of the algorithm at the expense of computation costs incurred by a large number of power operations.

Fig. 3 also reveals that Shades of Grey algorithm is more sensitive to the Minkowski norm than Grey-Edge and the proposed algorithms. This is mainly because Shades of Grey algorithm utilizes image intensity values directly, whereas Grey-Edge and the proposed algorithms operate on image details which are enhanced by the corresponding operators. Thus, the significant details can be easily enhanced with low values of Minkowski norm, whereas enhancing significant image intensity values requires larger values of Minkowski norm.

The best performances of the colour constancy algorithms on the controlled indoor dataset is shown in Table 1. The Minkowski norm and local smoothing operator used for Shades of Grey and Grey-Edge algorithms are set as $k = 6$ and $\sigma = 2$ to provide the best performance among all the possible combinations for the controlled indoor dataset. For the proposed algorithm, the wavelet filters are selected as Daubechies "db6" filters, and the same Minkowski norm of $k = 6$ is used. The 39% improvement in the performance of Shades of Grey algorithm over that of Grey-World algorithm is achieved at the expense of higher computational cost incurred by employing Minkowski norm of $k = 6$. Grey-Edge algorithm improves over the performance of Grey-World algorithm by 27%. This improvement is mainly due to the appropriate selection of the local smoothing operator σ and Minkowski norm k. However, its performance is not as good as Shades of Grey algorithm. This is because Grey-Edge algorithm depends mainly on edge information, and the dataset has samples which have weak edge information. Table 1 shows the proposed algorithm gives the best illuminant colour estimates. Again, a significant drop in the error is obtained by an appropriate choice of the Minkowski norm and wavelet filters. The proposed algorithm achieves 17% and 42% performance improvements over Shades of Grey and Grey-Edge algorithms, respectively. The improvements are mainly due to the multiscale structure of the estimation.

The performances of the proposed algorithm for different parameter settings is shown in Table 2 where the corresponding dependency graph is shown in Fig. 3(c). The worst performance of the proposed algorithm is with a median angular error of 5.24, which is significantly better than Grey-World and Max-RGB algorithms, and similar to the best performance of Grey-Edge algorithm. The worst performance is achieved with Minkowski norm of $k = 1$ and Daubechies wavelet filter of "db1". This indicates that the proposed algorithm with the basic settings of Minkowski norm of $k = 1$ and Daubechies wavelet filter of "db1" can produce results which are significantly better than that of Grey-World and Max-RGB algorithms, and comparable with that of the best performance provided by Grey-Edge algorithm. Thus the proposed algorithm outperforms the other algorithms on the controlled indoor dataset.

4.1.2. Real-World Dataset

The colour constancy algorithms are also evaluated on a dataset which represents a wide variation of typical indoor and outdoor scenes. The Grey Ball dataset [20] consists of 11,346 images extracted from fifteen video sequences, 6490 of which are outdoor scenes and 4856 are indoor scenes. A small grey sphere is placed at the bottom right corner of every scene and used as a colour reference. The sphere is used to estimate the scene illuminant colour. The estimated illuminant colours for all scenes are provided with the

Table 2: Performance of the proposed colour constancy algorithm in terms of median angular error (in degrees) against different parameters on the controlled indoor dataset.

Minkowski norm	Daubechies Wavelet Filter					
k	"db1"	"db2"	"db3"	"db4"	"db5"	"db6"
1	5.24	5.22	5.19	5.00	5.16	5.07
2	4.89	4.44	4.60	4.41	4.53	4.27
3	4.56	4.16	4.41	4.31	4.29	4.25
4	4.19	3.94	4.12	3.98	4.00	3.81
5	4.14	3.83	4.01	3.73	4.08	3.73
6	3.88	3.93	3.96	3.82	4.13	3.65

Figure 4: Sample images from the Grey Ball dataset [20].

database and are used as the ground truths in our experiments. Due to the high correlation among the images in a video sequence, the experiments are performed on a subset of 600 images corresponding to forty images from each of the fifteen video sequences. The pixels which encompass the grey sphere are excluded from the colour constancy computation. Some sample images from the Grey Ball dataset [20] are shown in Fig. 4.

The dependency of median error on different parameters of the algorithms on the Grey Ball dataset [20] is shown in Fig. 5. For Shades of Grey algorithm, the higher performances are achieved using larger values of the Minkowski norm (k). These are achieved with a tradeoff between performance and computational load. For Grey-Edge algorithm, the lower the values of Minkowski norm k and local smoothing operator σ, the better the performance. Similar to Grey-Edge algorithm, the lower values of Minkowski norm and length of Daubechies wavelet filters for the proposed algorithm provide the better performances. The similar performances of Grey-Edge and the proposed algorithms on the Grey Ball dataset are mainly because the image size in the dataset is relatively small which makes it difficult to detect significant image details with higher values of both local support σ for Grey-Edge algorithm and wavelet filter length for the proposed algorithm.

The best performances of the colour constancy algorithms on the Grey Ball dataset is shown in Table 3. For Shades of Grey algorithm, the Minkowski norm is set to $k = 6$. The Minkowski norm and local smoothing operator used for Grey-Edge algorithm are set as $k = 1$ and $\sigma = 1$ to provide the best performance among all the possible combinations on the controlled indoor dataset. For the proposed algorithm, the wavelet filters are selected as Daubechies "db1" filters, and the Minkowski norm of $k = 1$ is used. On average, Shades of Grey, Grey-Edge and the proposed algorithms have similar performances on the Grey Ball dataset. Their performances are significantly better than Grey-World and Max-RGB algorithms. The improvement provided by the proposed algorithm is mainly due to the adaptive illuminant colour estimation using the multiscale structure.

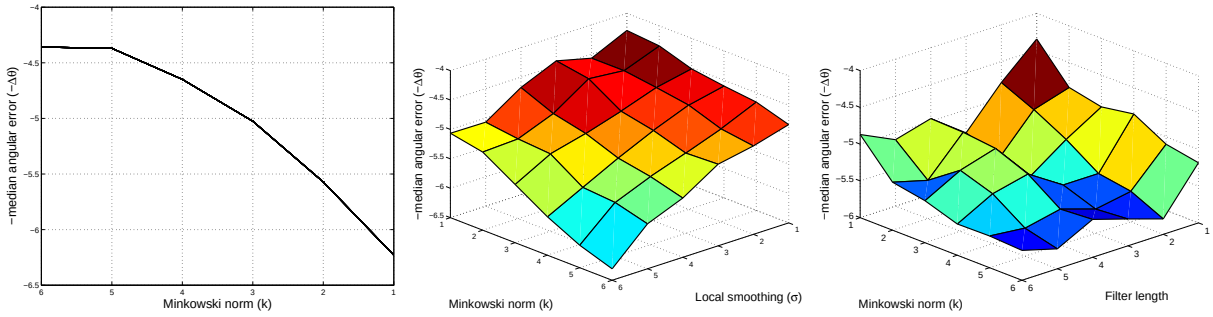

(a) (b) (c)

Figure 5: Dependency of median angular error on parameter settings of the colour constancy algorithms on the Grey Ball dataset [20]: (a) Shades of Grey; (b) Grey-Edge; and (c) the proposed algorithm. The angular error axis is inverted for visualization purpose. Since Shades of Grey algorithm is only dependent on Minkowski norm k, both the x- and y-axis of Shades of Grey graph refer to the Minkowski norm.

Table 3: Performances of different colour constancy algorithms in terms of median angular error (in degrees) on the Grey Ball dataset.

Method	Median Angular Error
Grey-World	6.23
Max-RGB	6.52
Shades of Grey	4.36
Grey-Edge	4.35
Proposed	4.29

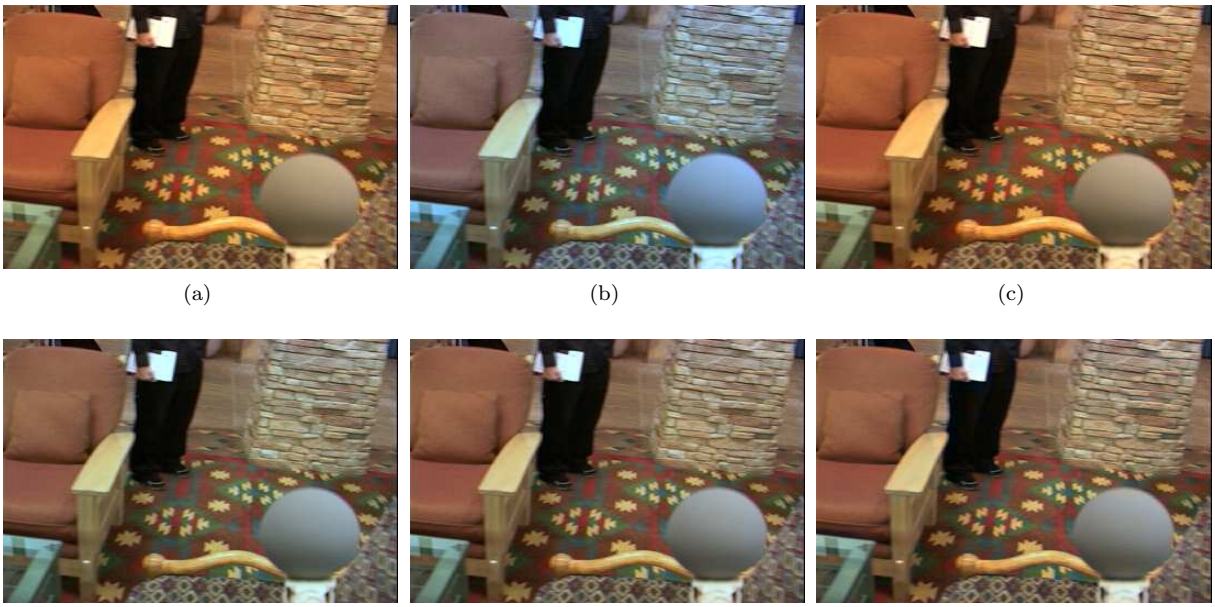

Figure 6: Colour constancy results and the corresponding angular errors between estimated and ground-truth illuminant colours using different algorithms on an input image from the Grey Ball dataset [20]. (a) Input image. Illuminant-colour corrected images obtained using: (b) Grey-World ($\Delta\theta = 9.5°$); (c) Max-RGB ($\Delta\theta = 8.0°$); (d) Shades of Grey ($\Delta\theta = 3.2°$); (e) Grey-Edge ($\Delta\theta = 1.1°$); and (f) proposed algorithm ($\Delta\theta = 0.6°$).

4.2. Qualitative Assessment

We also evaluate the performances of the different colour constancy algorithms subjectively. Sample images from the Grey Ball dataset are selected, and the optimum parameter settings for the best performances of the different algorithms reported in the previous section are used.

Fig. 6 shows the illuminant-colour images generated using Grey-World, Max-RGB, Shades of Grey, Grey-Edge and the proposed algorithms, and the corresponding angular errors between estimated and ground-truth illuminant colours. The colour of the image corrected by Grey-World algorithm is shifted toward blue, thus resulting in the highest angular error of $\Delta\theta = 9.5°$. The Max-RGB algorithm provides a minor improvement over Grey-World algorithm in terms of visual quality and angular error. Shades of Grey, Grey-Edge and proposed algorithms provide similar results in terms of visual quality. However, the best illuminant-colour corrected image is obtained using the proposed algorithm, which is supported by the lowest angular error value.

In Fig. 7, similar to Fig. 6, the result of Grey-World algorithm is shifted toward blue, and Max-RGB algorithm provides almost no improvement in terms of visual quality. Shades of Grey algorithm provides satisfactory results. However, the grey-coloured regions on the image is still perceived as blueish. This is apparent on the grey-coloured object around the bottom-left corner of the image. Grey-Edge algorithm provides a minor improvement. The proposed algorithm outperforms the other algorithms in terms of visual quality and the lowest angular error. Furthermore, the coloured regions in the resultant corrected image look natural.

In Fig. 8, Max-RGB algorithm provides the minimum angular error. This is an expected result because the white yacht is used as the reference colour in Max-RGB algorithm and the image correction is applied accordingly. The visual quality of the illuminant-colour corrected images of Grey-Edge and proposed algorithms are similar to that of Max-RGB algorithm. However, their angular errors are slightly higher. It is also clear that Grey-World and Shades of Grey algorithms provide the worst two performances in terms of visual quality and high angular errors.

(a) (b) (c)

(d) (e) (f)

Figure 7: Colour constancy results and the corresponding angular errors between estimated and ground-truth illuminant colours using different algorithms on an input image from the Grey Ball dataset [20]. (a) Input image. Illuminant-colour corrected images obtained using: (b) Grey-World ($\Delta\theta = 7.6°$); (c) Max-RGB ($\Delta\theta = 14.7°$); (d) Shades of Grey ($\Delta\theta = 3.0°$); (e) Grey-Edge ($\Delta\theta = 8.1°$); and (f) proposed algorithm ($\Delta\theta = 1.6°$).

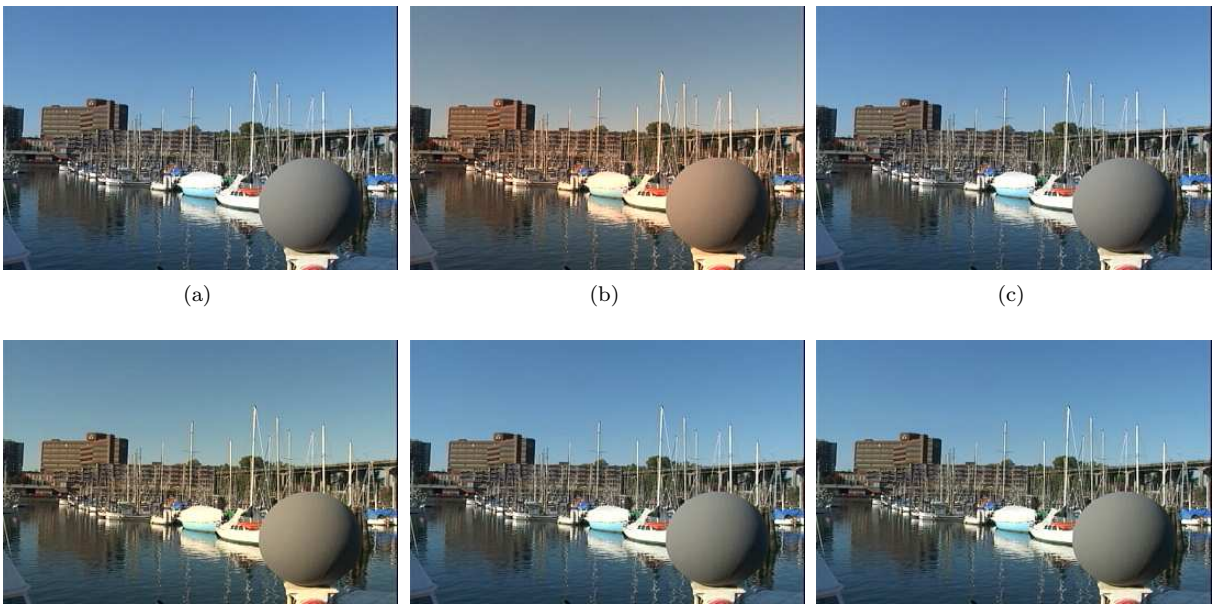

(a) (b) (c)

(d) (e) (f)

Figure 8: Colour constancy results and the corresponding angular errors between estimated and ground-truth illuminant colours using different algorithms on an input image from the Grey Ball dataset [20]. (a) Input image. Illuminant-colour corrected images obtained using: (b) Grey-World ($\Delta\theta = 9.8°$); (c) Max-RGB ($\Delta\theta = 1.5°$); (d) Shades of Grey ($\Delta\theta = 6.4°$); (e) Grey-Edge ($\Delta\theta = 2.3°$); and (f) proposed algorithm ($\Delta\theta = 2.2°$).

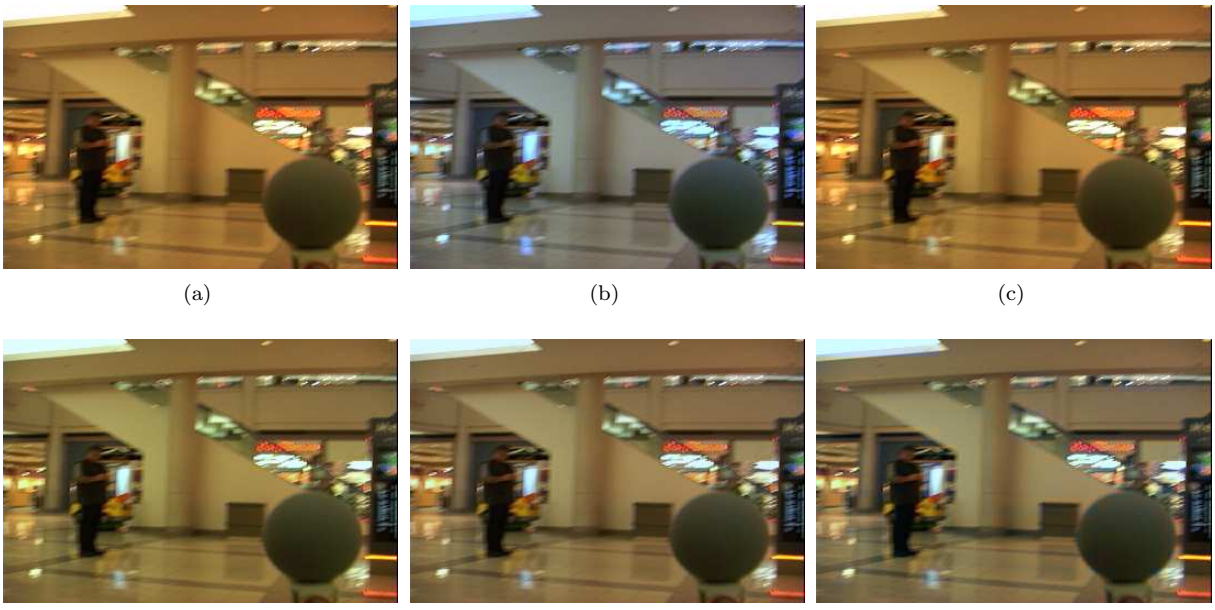

(a) (b) (c)

(d) (e) (f)

Figure 9: Colour constancy results and the corresponding angular errors between estimated and ground-truth illuminant colours using different algorithms on an input image from the Grey Ball dataset [20]. (a) Input image. Illuminant-colour corrected images obtained using: (b) Grey-World ($\Delta\theta = 4.3°$); (c) Max-RGB ($\Delta\theta = 10.6°$); (d) Shades of Grey ($\Delta\theta = 10.9°$); (e) Grey-Edge ($\Delta\theta = 7.3°$); and (f) proposed algorithm ($\Delta\theta = 4.9°$).

Finally, Fig. 9 shows the performances of the colour constancy algorithms on an image containing highly specular objects. The best performance is provided by Grey-World algorithm with an angular error of $\Delta\theta = 4.3°$. Max-RGB algorithm fails to provide a satisfactory result since it recognises the specular objects as white objects. Similar to Max-RGB algorithm, Shades of Grey and Grey-Edge algorithms also fail to estimate the correct illuminant colour. The proposed algorithm achieves an angular error of $\Delta\theta = 4.9°$, which is so close to that of Grey-World algorithm. However, when the results are compared visually, the colour of the image corrected by Grey-World algorithm is slightly shifted toward blue, which is not the case for the result of the proposed algorithm. Further results of the proposed algorithm on sample pictures from Kodak's "Picture of the Day" dataset are shown in Fig. 10.

The proposed algorithm employs DWT and Minkowski norm to estimate the illuminant colour. Thus it's computational cost mainly depends on the image size and the degree of the Minkowski norm. The larger the size of the image and/or the higher the degree of Minkowski norm, the higher the computational cost is. The algorithm is implemented in MATLAB on a PC with 2-GHz Intel(R) Core(TM)2 Duo CPU, and 2-GB RAM. It takes less than 100 ms to process a colour image of size 350×350 pixels with the basic settings of Minkowski norm of $k = 1$ and Daubechies wavelet filter of "db1". The computational cost can be further reduced if the DWT is computed at hardware level, and a look-up table is used in computing Minkowski norm.

5. Conclusions

In this paper we propose a colour constancy algorithm which benefits from the DWT multiscale decomposition of an input colour image. The adaptiveness of the algorithm is achieved by using the angular error between estimated illuminant colours in consecutive scales to determine the optimum scale for the best estimate of the true illuminant colour. The inverse DWT of the wavelet and approximation subbands modified according to the estimated illuminant colour of the colour image channels generates the illuminant-colour

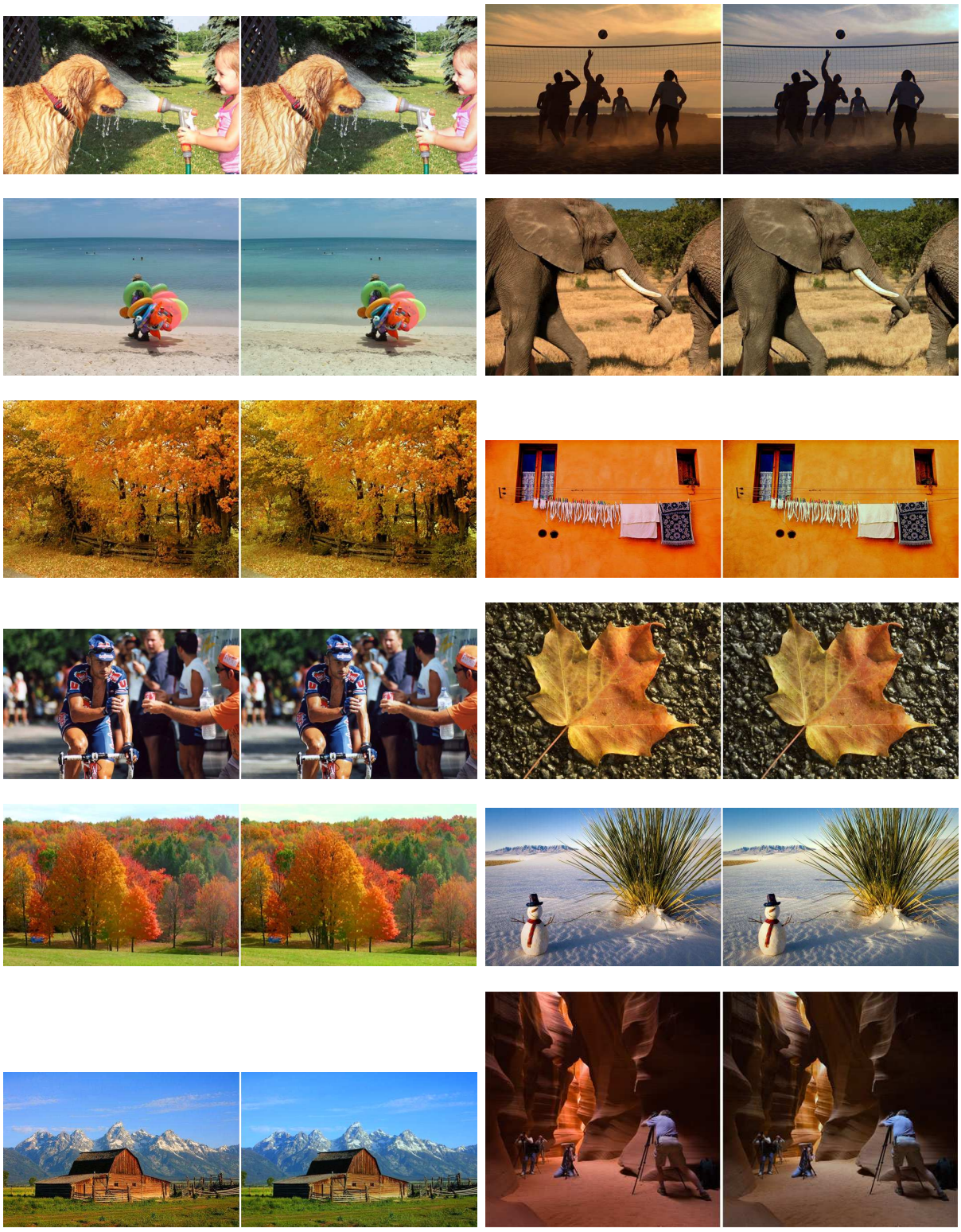

Figure 10: Results of the proposed algorithm on sample images from Kodak's "Picture of the Day" dataset. For each pair or images, the left and right ones are referring to the original and the processed images, respectively.

corrected image. Since the proposed algorithm uses low level image features, it is of much lesser complexity than gamut mapping and GCIE algorithm. It does not require a dataset with known illuminant colour for calibration.

Using test images of indoor and outdoor scenes, the proposed algorithm has been shown, both quantitatively and subjectively, to produce colour constancy results at least comparable and mostly better than those produced by four state-of-the-art colour constancy algorithms of similar complexity. The performances are evaluated in term of accuracy of the estimated illuminant colours and visual quality of the illuminant-colour corrected images obtained by the different algorithms.

The colour constancy framework can be easily applied in real-time since hardware implementation of DWT decomposition and reconstruction are widely available. Thus it can be easily adapted to real-time applications which requires colour constancy, such as JPEG2000. As a future work, it is worth exploring the application of the proposed framework to other multiscale transforms such as ridgelet and curvelet. Furthermore, it will be useful to determine the performances of the proposed framework using different wavelet filters so as to determine the wavelet filter set which gives the best performance.

References

[1] M. Ebner, Color Constancy, 1st Edition, Wiley Publishing, 2007.

[2] K. Barnard, V. Cardei, B. Funt, A comparison of computational color constancy algorithms. i: Methodology and experiments with synthesized data, IEEE Transactions on Image Processing 11 (9) (2002) 972–984.

[3] J.-M. Geusebroek, R. van den Boomgaard, A. Smeulders, H. Geerts, Color invariance, IEEE Transactions on Pattern Analysis and Machine Intelligence 23 (12) (2001) 1338–1350.

[4] G. Finlayson, S. Hordley, P. HubeL, Color by correlation: a simple, unifying framework for color constancy, IEEE Transactions on Pattern Analysis and Machine Intelligence 23 (11) (2001) 1209–1221.

[5] D. H. Brainard, W. T. Freeman, Bayesian color constancy, The Journal of the Optical Society of America A 14 (7) (1997) 1393–1411.

[6] V. C. Cardei, B. Funt, K. Barnard, Estimating the scene illumination chromaticity by using a neural network, The Journal of the Optical Society of America A 19 (12) (2002) 2374–2386.

[7] P. V. Gehler, C. Rother, A. Blake, T. Minka, T. Sharp, Bayesian color constancy revisited, in: Proceedings of IEEE Conference on Computer Vision and Pattern Recognition, 2008, pp. 1–8.

[8] D. A. Forsyth, A novel algorithm for color constancy, International Journal of Computer Vision 5 (1) (1990) 5–36.

[9] G. D. Finlayson, S. D. Hordley, Gamut constrained illuminant estimation, International Journal of Computer Vision 67 (1) (2006) 93–109.

[10] J. van de Weijer, T. Gevers, A. Gijsenij, Edge-based color constancy, IEEE Transactions on Image Processing 16 (9) (2007) 2207–2214.

[11] K. Barnard, L. Martin, A. Coath, B. Funt, A comparison of computational color constancy algorithms. ii. experiments with image data, IEEE Transactions on Image Processing 11 (9) (2002) 985–996.

[12] E. H. Land, J. J. McCANN, Lightness and retinex theory, The Journal of the Optical Society of America A 61 (1) (1971) 1–11.

[13] G. Buchsbaum, A spatial processor model for object colour perception, Journal of the Franklin Institute 310 (1980) 1–26.

[14] G. Finlayson, E. Trezzi, Shades of gray and colour constancy, in: Proceedings of IS&T/SID Twelfth Color Imaging Conference, 2004, pp. 37–41.

[15] M. Ebner, G. Tischler, J. Albert, Integrating color constancy into jpeg2000, IEEE Transactions on Image Processing 16 (11) (2007) 2697–2706.

[16] I. Daubechies, Ten lectures on wavelets, Society for Industrial and Applied Mathematics, Philadelphia, PA, USA, 1992.

[17] S. Mallat, A Wavelet Tour of Signal Processing, Third Edition: The Sparse Way, Academic Press, 2008.

[18] S. D. Hordley, G. D. Finlayson, Reevaluation of color constancy algorithm performance, The Journal of the Optical Society of America A 23 (5) (2006) 1008–1020.

[19] K. Barnard, L. Martin, B. Funt, A. Coath, A data set for color research, Color Research and Application 27 (3) (2002) 148–152.

[20] F. Ciurea, B. Funt, A large image database for color constancy research, in: Proceedings of IS&T/SID Eleventh Color Imaging Conference, 2003, pp. 160–164.